Supplemental notes for: "Non-gaussian spatial correlations dramatically weaken localization"

H. Javan Mard,[1] E. C. Andrade,[2] E. Miranda,[3] and V. Dobrosavljević[1]

[1] *Department of Physics and National High Magnetic Field Laboratory, Florida State University, Tallahassee, FL 32306*
[2] *Institut für Theoretische Physik, Technische Universität Dresden, 01062 Dresden, Germany*
[3] *Instituto de Física Gleb Wataghin, Unicamp, R. Sérgio Buarque de Holanda, 777, Campinas, SP 13083-859, Brazil*

(Dated: September 22, 2014)

PACS numbers:

I. COMPUTATION OF THE CONDUCTANCE

The dimensionless conductance computed in this work is defined as $g = G/\left(2e^2/h\right)$. The sample conductance g_s, with the effects of the contacts already removed, is given by the Landauer relation [1]

$$g_s = \frac{< T_s >_{typ}}{1- < T_s >_{typ}}, \quad (1)$$

where T_s is the total sample transmittance, and 'typ' refers to the geometrical average $< T_s >_{typ} = \exp \overline{\ln T_s}$ (the overbar denoting an average over realizations). The transmission function is simply given by [2]

$$T(\omega) = \frac{1}{2}\mathrm{Tr}\left[\mathbf{G}_S^{\dagger}(\omega)\,\mathbf{\Gamma}_R(\omega)\,\mathbf{G}_S(\omega)\,\mathbf{\Gamma}_L(\omega)\right]. \quad (2)$$

Here, all bold-face quantities are matrices in the lattice site basis, and ω is set to zero in our case, representing the Fermi level $T = 0$. $\mathbf{\Gamma}_{L(R)}(\omega)$ are the coupling matrices, describing the coupling of the system to non-interacting left (L) and right (R) leads, and are determined by the leads' self-energies as

$$\mathbf{\Gamma}_{L(R)}(\omega) = i\left(\mathbf{\Sigma}_{L(R)} - \mathbf{\Sigma}_{L(R)}^{\dagger}\right). \quad (3)$$

For the sake of simplicity, we assume

$$\mathbf{\Sigma}_{L(R)} = -i\eta\mathbf{B}_{L(R)}, \quad (4)$$

where the matrix $\mathbf{B}_{L(R)}$ is equal to 1 for a site i connected to the left (right) lead and 0 otherwise. This constant lead self-energy is equivalent to the assumption of wide lead bands. $\mathbf{G}_S$ is the sample Green's function, given by

$$\mathbf{G}_S = \left[(\omega+\mu)\,\mathbf{1} - \mathbf{H}_S^0 - \mathbf{\Sigma}_S - \mathbf{\Sigma}_L - \mathbf{\Sigma}_R\right]^{-1}, \quad (5)$$

where μ is the chemical potential. $\mathbf{H}_S^0$ is the non-interacting sample Hamiltonian and $\mathbf{\Sigma}_S$ is the sample self-energy, which accounts for the electronic correlations. As we employ a Hartree-Fock approach, the sample self-energy is given by

$$\mathbf{\Sigma}_S = \frac{U}{2}\langle\mathbf{n}\rangle + \mu\mathbf{1}. \quad (6)$$

$\mathbf{n}$ is a diagonal matrix in the site basis whose elements n_i correspond to the occupation of the site i. It can be seen from Eqs. (5), (6) and (4) that the sample Green's function can be obtained through a single diagonalization of an effective Hamiltonian, as opposed to a matrix inversion for every frequency value. Even with this simplification, we are still left with a non-Hermitian matrix. We have implemented this diagonalization step using standard LAPACK routines. A particular efficient implementation can be achieved using the OpenMP version of Intel's MKL library, which allowed us to perform these calculations on a desktop computer. Furthermore, using Eqs. (3) and (4), we can rewrite Eq. (2) as

$$T(\omega) = 2\eta^2\mathrm{Tr}\left[\mathbf{G}_{1L}(\omega)\,\mathbf{G}_{L1}^{\dagger}(\omega)\right], \quad (7)$$

where $\mathbf{G}_{1L}(\omega)$ is the sample Green's function from the first site ($i = 1$) (connected to the left lead) to the last one ($i = L$) (connected to the right lead).

II. THE LOCALIZATION LENGTH

The localization length ξ is calculated using the exponential behavior of the conductance (e^{-x}) at very large $x = \frac{L}{\xi}$ (for this, either L or W should be very large). In other words, it can be computed from the slope of the conductance as a function of x on a semi-log scale (assuming all states are localized, which we always find). Fig. 1 shows that adding interactions considerably increases the localization length, even though all states remain localized.

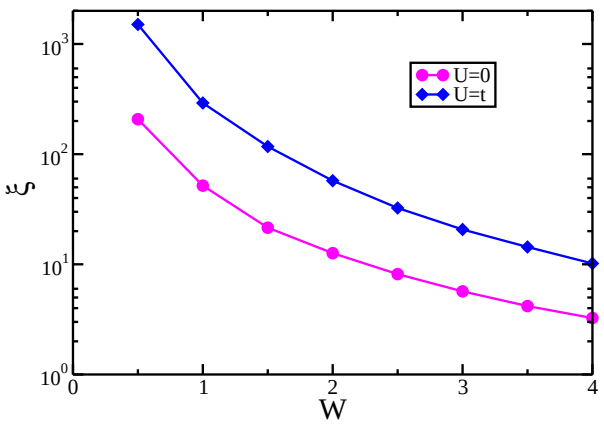

Figure 1: (Color online) Localization length ξ as a function of W obtained from the collapse of the conductance curves. ξ is strongly enhanced for $U = t$, even though all states remain localized.

III. OPERATIONAL DEFINITION OF THE CHARACTERISTIC CONDUCTANCE

We now show that the characteristic conductance g^* can be determined in practice as the value at the point $L = L^* = (\ln 2)\xi$, or $x = \ln 2$. Given the beta function for 1D localization, we can write

$$\ln \frac{L}{L_0} = \int_{g_0}^{g} \frac{d\ln g}{\beta(g)} = F(g) - F(g_0), \tag{8}$$

where we define the function

$$F(g) \equiv \int^{g} \frac{d\ln g}{\beta(g)}, \tag{9}$$

and g_0 is a reference conductance at scale L_0. From Eq. (8) we get

$$F[g(L)] = \ln\left[\frac{Le^{F(g_0)}}{L_0}\right], \tag{10}$$

which implicitly gives $g(L)$. Defining the reference conductance $g = g^*$ at $L = L^*$

$$F[g(L)] = \ln\left(\frac{Le^{F(g^*)}}{L^*}\right). \tag{11}$$

Using the form proposed in the main text $\beta(g) = \beta_0(g/g^*)$ and the non-interacting beta function of ref. 3, we find

$$F(g) = -\int^{g} \frac{d\ln g}{\left(1+\frac{g}{g^*}\right)\ln\left(1+\frac{g^*}{g}\right)} = \ln\left[B\ln\left(1+\frac{g^*}{g}\right)\right], \tag{12}$$

where B is an arbitrary constant. It then follows from Eq. (11) that

$$F(g) = \ln(\frac{L}{L^*}B\ln 2). \tag{13}$$

On the other hand, the scaling function proposed in ref. 3 is

$$\frac{g^*}{g} = e^{L/\xi} - 1, \tag{14}$$

which, when plugged into Eq. (12), leads to

$$F(g) = \ln[B\frac{L}{\xi}]. \tag{15}$$

Finally, comparing Eqs. (13) and (15) gives us the anticipated result $L^* = (\ln 2)\xi \approx 0.69\xi$.

IV. SPATIAL CORRELATIONS OF THE RENORMALIZED DISORDER POTENTIAL

A. Weak disorder

An important question is how to characterize the spatial correlations between the renormalized site energies v_i. For weak disorder, this problem is solvable analytically. Expanding the average on the right-hand side of Eq. (2) of the main text to first order in the bare disorder, we find the spatial Fourier component [4, 5]

$$v_q = \frac{\varepsilon_q}{1 - U\Pi_q} + O(\varepsilon_q^2), \tag{16}$$

where Π_q is the usual static Lindhard polarization function of the clean, non-interacting system, which in the case of a one-dimensional tight-binding chain is given by

$$\Pi_q = -\rho(\varepsilon_F)\frac{1}{\sin(q/2)}\ln\left[\frac{\cos(q/2)}{1-\sin(q/2)}\right], \tag{17}$$

where $\rho(\varepsilon_F)$ is the density of states at the Fermi level.

Using Eqs. (16) and (17) we can generate a renormalized potential v_i in this linear response approach (LRA). The result of this procedure is shown in Fig. 2. As can be seen from Fig. 2, although the LRA potential exhibits both disorder screening and spatial correlations, it does not capture the renormalization of g^*: the scaling function (and its mathematical equivalent, the beta function) coincides with the one from the non-interacting calculation. This result strongly suggests that the g^* renormalization is a *non-perturbative* effect of disorder and a fully self-consistent solution is needed in order to capture it.

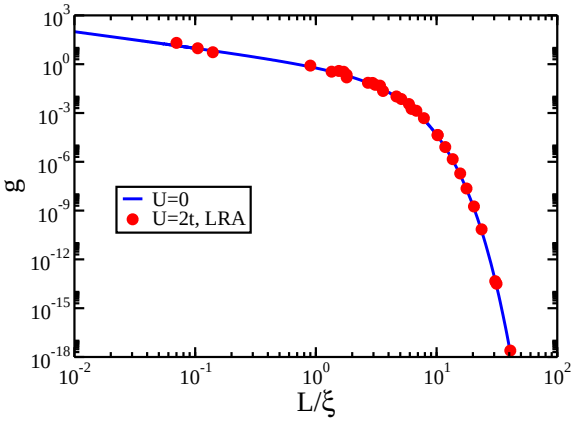

Figure 2: (Color online) The scaling function in the linear response approach compared with the non-interacting one.

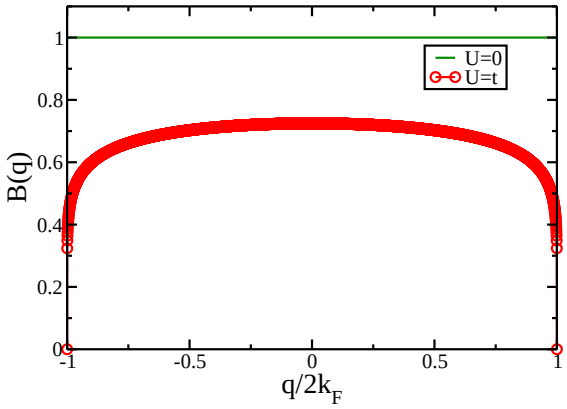

Figure 4: (Color online) Fourier transform of the two point correlation function B_{ij} for $W = 2t$ and $U = t$.

B. Gaussian correlations

To go beyond the weak disorder limit, we calculate the fully self-consistent HF two-point correlation function $\langle v_i v_j \rangle$. Here $\langle \cdots \rangle$ denotes an average over both pairs and disorder realizations. This function only depends on the distance $r = r_i - r_j$ between the two sites. In Fig. 3 we show $B(r) = \langle v_i v_j \rangle / W_{eff}^2$ as a function of the distance r between two sites. W_{eff} is the effective disorder width, which is simply given by the standard deviation of v_i. Defined in this fashion, $B(r = 0) = 1$. It displays Friedel-like oscillations which are enhanced as U increases. For comparison, we also show $B(r)$ obtained within LRA at $U = t$.

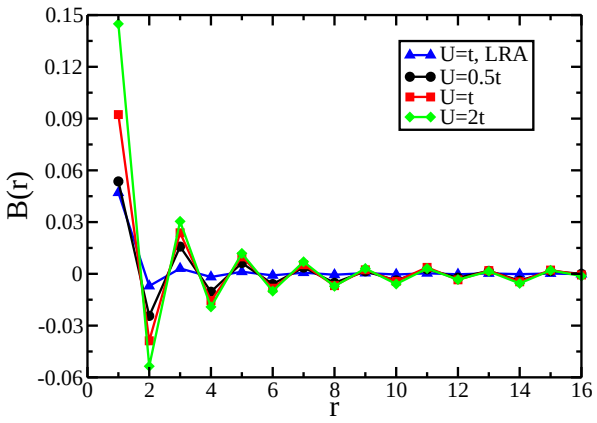

Figure 3: (Color online) Spatial pair correlations between the renormalized site energies for $W = 1.0t$ and $L = 400$.

Since a Gaussian distribution is fully determined by its two-point correlation function, we can use $\langle v_i v_j \rangle$ to generate Gaussian correlated variables. More precisely, we generated v_i deviates obeying a multivariate Gaussian distribution with zero mean and covariance matrix $\langle v_i v_j \rangle$. To do this, we first calculate the Fourier transform of B_{ij}, $B(q)$, which is shown in Fig. 4. As expected, its derivative diverges at $q = \pm 2k_F$, giving rise to long-ranged Friedel-like oscillations, as shown in Fig. 3. Once we have $B(q)$, we generate Gaussian distributed random complex numbers v_q using the Box-Muller method with zero mean and a q-dependent variance $W_{eff}^2 B(q)$ [6]. Note that each v_q obeys a univariate Gaussian distribution. We can then obtain their real space values v_i after a numerical Fourier transform.

The result of this procedure is shown in the main text, where it is shown to be insufficient to capture both the renormalization of the crossover scale g^* and the enhancement of the localization length (see Fig. 5). Therefore, we conclude that this phenomenon is not only non-perturbative in disorder but also determined by higher order disorder correlations beyond the Gaussian level.

C. Full characterization of inter-site correlations

In order to characterize the behavior of the inter-site correlations, we focus on the distribution function of two given sites i and j. Evidently, this distribution only depends on the distance between sites $|i - j| = r$, so we will denote it by $P_r^{(2)}(v_i \equiv x, v_j \equiv y)$. If there were no inter-site correlations, then we would have

$$P_r^{(2)}(x, y) = P^{(1)}(x) P^{(1)}(y), \tag{18}$$

where $P^{(1)}(v_i \equiv x)$ is the distribution of renormalized site energies of a given site. Both distributions were ob-

tained numerically from our calculations. In Fig. 6 we show the ratio of the left-hand and the right-hand sides of Eq. (18) for $r = 1$. The fact that it is not equal to 1 is a demonstration of the existence of inter-site correlations.

Further insight can be gained by noting that if Eq. (18) were true, then $P_r^{(2)}(x, y)$ would symmetric with respect to the interchange of its arguments. That this is not the case is made clear by a glance at a color scale plot of $P_r^{(2)}(x, y)$ in the xy plane, as shown in Fig. 7 for $r = 1$. In fact, this anisotropy suggests a simple parametrization of the distributions.

We first notice that the $P^{(1)}(x)$ can be very accurately captured by the following two-parameter function if the bare disorder is uniform

$$Q^{(1)}(x) = \frac{1/\widetilde{W}}{1 + \exp\left[\left(|x| - \widetilde{W}/2\right)/\delta\widetilde{W}\right]}. \qquad (19)$$

Here, $\widetilde{W}$ is the effective renormalized disorder and $\delta\widetilde{W}$ rounds the tails of the distribution. Fig. 8 shows the raw numerical data compared to the best fit using Eq. (19). The agreement is excellent.

We then propose a single-parameter function for the two-site distribution

$$Q_r^{(2)}(x, y) = Q^{(1)}(x')\, Q^{(1)}(y'), \qquad (20)$$

where

$$\begin{cases} x' &= \frac{1}{1-c^2}x - \frac{c}{1-c^2}y, \\ y' &= \frac{-c}{1-c^2}x + \frac{1}{1-c^2}y, \end{cases} \qquad (21)$$

and c is the anisotropy parameter. The above transformation represents a stretch along the main diagonal and a shrinking along the secondary diagonal. An excellent description of the data is obtained with Eq. (20).

Therefore, we can parametrize the two-site correlations by the single parameter c. The dependence of c on r is shown in Fig. 10, where we see a gradual decrease of correlations with the distance between the two sites. This reduction is well fitted by a straight line and our results are consistent with $c \to 0$ as $r \to \infty$.

Since the most important inter-site correlations are for nearest-neighbor sites, we have generated random site energies distributed according to $P_1^{(2)}(x, y)$, thus neglecting correlations for $r > 1$. We then calculated the corresponding conductance, which we call g_{nn}, 'nn' here highlighting the fact that it contains the effects of the *exact* correlations up to nearest neighbors.

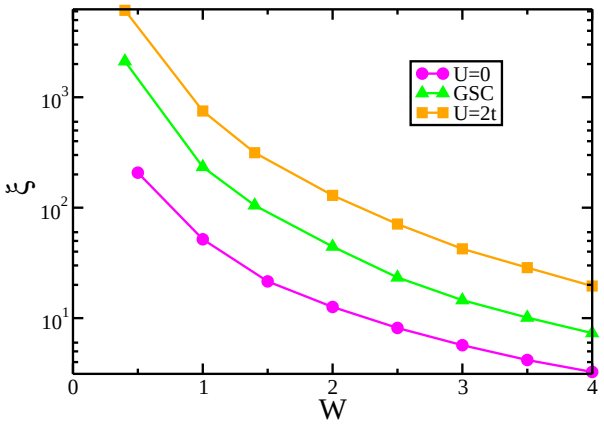

Figure 5: (Color online) Localization length ξ as a function of W, obtained from the collapse of the conductance curves. We see that ξ is enhanced if we retain only Gaussian correlations of the site energies (GSC), but not as strongly as to be able to reproduce the complete HF results.

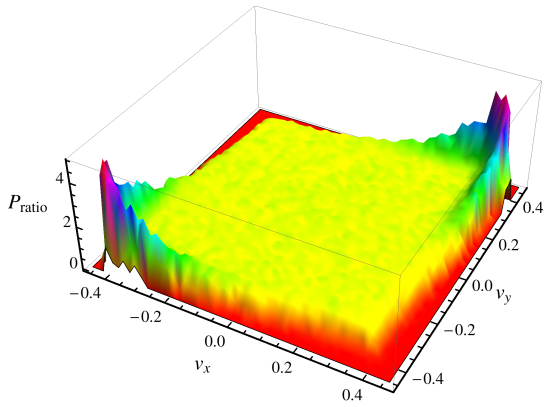

Figure 6: (Color online) The ratio of distributions $P_{ratio}(x, y) = P_1^{(2)}(x, y)/P^{(1)}(x)\,P^{(1)}(y)$ for $U = W = t$, and $L = 10^3$ with 1,000 realizations of disorder. Deviations from 1 are indications of inter-site correlations.

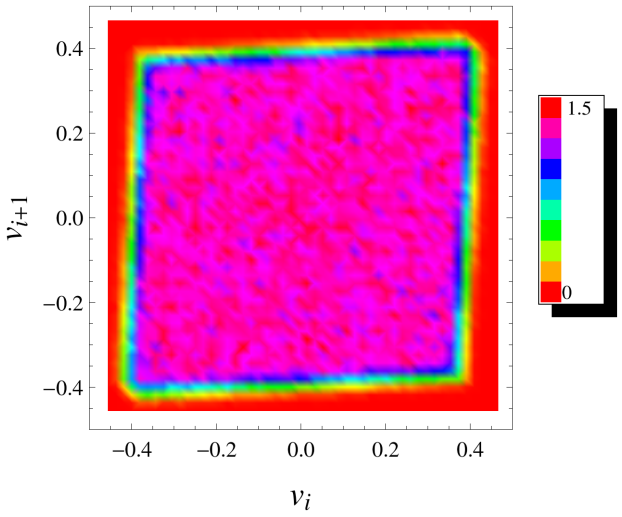

Figure 7: (Color online) The color scale plot of $P_1^{(2)}(x, y)$ for $U = W = t$, and $L = 10^3$ with 1,000 realizations of disorder. The strong anisotropy reflects the presence of appreciable inter-site correlations.

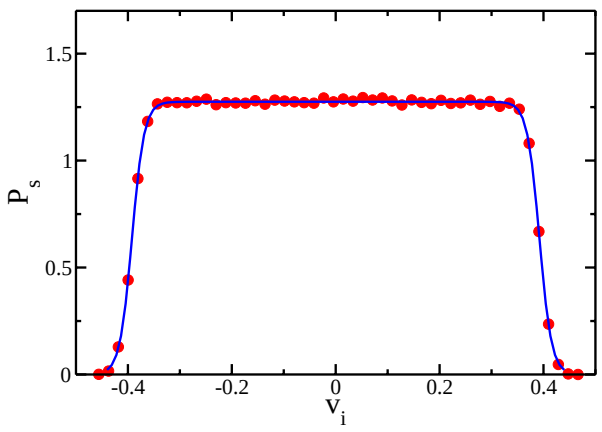

Figure 8: (Color online) The histogram of single site energy, $P(v_i)$, is well fitted to a Fermi-Dirac like distribution. The solid line is the fitted function described by Eq. 19 with two parameters $\widetilde{W} = 0.3921 \pm 0.0002$, and $\delta\widetilde{W} = 0.01172 \pm 0.0001$. Here $U = W = t$, and $L = 1000$.

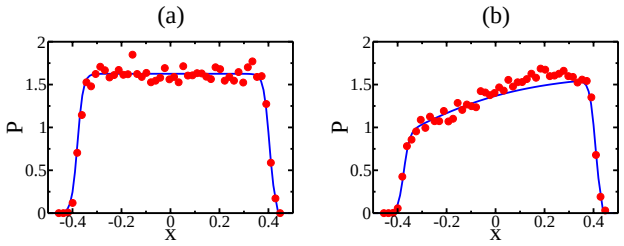

Figure 9: The proposed function $Q^{(2)}_{r=1}(x, y)$ (blue lines) compared to the raw data (red dots) for fixed values of y: (a) $y = 0.27$ and (b) $y = 0.37$.

The scaling plot of g_{nn} is shown as the red circles in Fig. 11. We have fitted the data points to the rescaled conductance of Eq. (14) (dashed blue line). For comparison, we have also plotted the corresponding scaling curves of the full (slave boson) calculation (dotted red line) and of the non-interacting case (continuous black line). The characteristic conductance of g_{nn} is $g^* = 0.72$, which is significantly different from the non-interacting value of 1, even though it is still larger than the full value of 0.18. Clearly, inter-site correlations are responsible for the suppression of g^*. Naturally, spatial correlations with $r > 1$ should to be taken into account to recover the full value of g^*.

As advertised at the beginning of this section, our results show that the spatial correlations among the renormalized site energies v_i are large for $r = 1$. Novel effects coming from a short-ranged form of inter-site correlations of the screened disorder potential have been discussed in the literature before, for instance in the context of the random dimer model [7], where the presence of extended

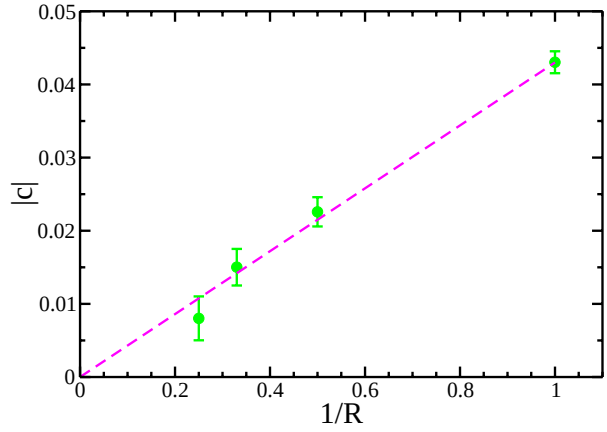

Figure 10: (Color online) The anisotropy parameter c as a function of the inter-site distance. The dashed line fit is $|c| = \alpha/R$, where $\alpha = 0.045 \pm 0.003$. Here $U = W = t$, and $L = 1000$.

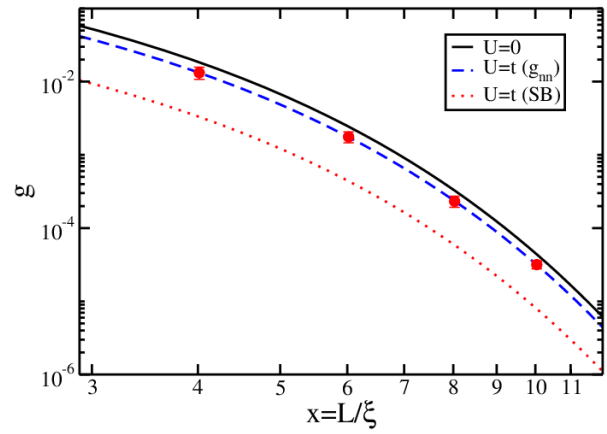

Figure 11: (Color online) The scaling plot of g_{nn} (see text) as a function of $x = L/\xi$ for $U = t$ (red circles), fitted to the scaling function of Eq. (14) (dashed blue line), with characteristic conductance $g^* = 0.72$. Also shown are the scaling functions for the non-interacting case ($g^* = 0$, continuous black line) and for the full slave boson results at $U = t$ ($g^* = 0.18$, dotted red line). The localization length ξ was obtained form the exponential behavior at large system sizes ($g \propto \exp(-L/\xi)$).

states in $1D$ is firmly established [7]. Even though our model does not show extended states, the renormalization of g^* translates into a delay in the crossover from extended to the localized states, strongly hinting towards a link between inter-site correlations and the robustness of extended states in disordered electronic systems.

[1] P. Markoš, Acta Phys. Slovaca **51**, 581 (2006).
[2] H. Haug and A. P. Jauho, *Quantum Kinetics in Transport and Optics of Semiconductors*, 1st ed. (Springer-Verlag, 1996).
[3] P. Anderson, D. Thouless, E. Abrahams, and D. Fisher, Phys. Rev. B **22**, 3519 (1980).
[4] E. C. Andrade, E. Miranda, and V. Dobrosavljević, Phys. Rev. Lett. **104**, 236401 (2010).
[5] E. C. Andrade, E. Miranda, and V. Dobrosavljević, J. Supercond. Nov. Magn. **25**, 1399 (2012).
[6] G. E. P. Box and M. E. Muller, Ann. Math. Stat. **29**, 610 (1958).
[7] D. H. Dunlap, H.-L. Wu, and P. W. Phillips, Phys. Rev. Lett. **65**, 88 (1990).